



ELSEVIER

Applied Mathematical Modelling 26 (2002) 449–472

APPLIED  
MATHEMATICAL  
MODELLING

[www.elsevier.com/locate/apm](http://www.elsevier.com/locate/apm)

# A numerical and experimental investigation of the modeling of microwave heating for liquid layers using a rectangular wave guide (effects of natural convection and dielectric properties)

P. Ratanadecho <sup>\*,1</sup>, K. Aoki <sup>2</sup>, M. Akahori <sup>3</sup>

*Department of Mechanical Engineering, Nagaoka University of Technology, 1603-1, Kamitomioka, Nagaoka,  
Niigata 940-2188, Japan*

Received 21 August 2000; received in revised form 22 March 2001; accepted 4 May 2001

---

## Abstract

The heating of a liquid layer by microwave with a rectangular wave guide has been investigated numerically and experimentally. It was performed for two different liquid layers: water layer and NaCl-water solution layer. A complete mathematical model is proposed, which uses comprehensive two-dimensional heat and momentum equations to describe unsteady temperature and fluid flow fields, coupled with a complete solution of the unsteady Maxwell's equations in the time domain can be used to investigate many aspects of the heating process. In this work, the effects of electric conductivity (which corresponds to the percentage by weight of NaCl in liquid layer) and microwave power level on the heating process were examined. Based on a model combining the Maxwell and heat transport and fluid flow equations, the results show that the heating kinetic strongly depends on the dielectric properties. © 2002 Elsevier Science Inc. All rights reserved.

**Keywords:** Microwave heating; Rectangular wave guide; Convection; Liquid layer; Dielectric properties

---

<sup>\*</sup> Corresponding author.

E-mail address: [phadu@blue.nagaokaut.ac.jp](mailto:phadu@blue.nagaokaut.ac.jp) (P. Ratanadecho).

<sup>1</sup> Ph.D. student.

<sup>2</sup> Professor of the Mechanical Engineering Department.

<sup>3</sup> Research Associate.

## Nomenclature

$A$	area ( $\text{m}^2$ )
$B$	magnetic flux density ( $\text{Wb}/\text{m}^2$ )
$C_p$	specific heat capacity ( $\text{J}/(\text{kg K})$ )
$D$	electric flux density ( $\text{C}/\text{m}^2$ )
$E$	electric field intensity ( $\text{V}/\text{m}$ )
$f$	frequency of incident wave (Hz)
$g$	gravitational constant ( $\text{m}/\text{s}^2$ )
$H$	magnetic field intensity ( $\text{A}/\text{m}$ )
$J$	current density ( $\text{A}/\text{m}^2$ )
$L$	length of a rectangular wave guide (m)
$P$	power (W)
$p$	pressure (Pa)
$q$	electric charge density ( $\text{C}/\text{m}^3$ )
$Q$	local electromagnetic heat generation term ( $\text{W}/\text{m}^3$ )
$S$	Poynting vector ( $\text{W}/\text{m}^2$ )
$T$	temperature ( $^\circ\text{C}$ )
$t$	time (s)
$\tan \delta$	dielectric loss coefficient (dimensionless)
$u, w$	velocity component (m/s)
$Z_H$	wave impedance ( $\Omega$ )
$Z_I$	intrinsic impedance ( $\Omega$ )

### Greek letters

$\alpha$	thermal diffusivity ( $\text{m}^2/\text{s}$ )
$\beta$	coefficient of thermal expansion (1/K)
$\eta$	absolute viscosity (Pa s)
$\varepsilon$	permittivity (F/m)
$\lambda$	wavelength (m)
$\mu$	magnetic permeability (H/m)
$v$	velocity of propagation (m/s)
$\nu$	kinematics viscosity ( $\text{m}^2/\text{s}$ )
$\rho$	density ( $\text{kg}/\text{m}^3$ )
$\sigma$	electric conductivity (S/m)
$\omega$	angular frequency (rad/s)
$\xi$	surface tension (N/m)

### Subscripts

$\infty$	ambient condition
a	air
j	layer number
in	input

r	relative
w	water
$x, y, z$	coordinates
0	free space, initial condition
<i>Superscripts</i>	
'	one of the different materials
*	complex conjugate

## 1. Introduction

Microwave heating is one of the most interesting methods for heating materials. Unlike other heat sources such as conventional heating, where heat is applied externally to the surface of the material, microwave irradiation penetrates and simultaneously heats the bulk of the material.

Microwave technology has several advantages over conventional methods, such as minimizing the heating times, uniform temperature distribution, high energy efficiency, and offers improvements in product quality for various industrial applications. Many successful examples of this application include the drying of foods, drying of textiles, freeze drying process, and vulcanization of rubber.

Refer to Metaxas and Meredith [1] and Saltiel and Datta [2] for an introduction to heat and mass transfers in microwave processing. A number of other analyses of the microwave heating process have appeared in the recent literature [3–11].

Although most of the previous investigations considered simulations of microwave heating in a solid sample, a little effort has been reported on the study of multi-dimensional heating process of the liquid layer by microwave fields, especially, a full comparison between mathematical simulated results with experimental heating data.

A study of the natural convection in a liquid exposed to microwave was studied by Saltiel and Datta [2] and Ayappa and Brandon [12] which the microwave power absorbed was assumed to decay exponentially into the sample following the aid of Lambert's law. However, this assumption is valid only for the large sample dimensions and high loss dielectric materials [13]. For small samples, or low loss dielectric sample, the spatial variations of electromagnetic fields and microwave power absorbed within samples must be required by a complete solution of the unsteady Maxwell's equations.

Due to the limited amount of theoretical and experimental work on microwave heating of liquid layer reported to date, the various effects are not fully understood and a number of critical issues remain unresolved. These effects of the reflection rate of microwave, the variation of microwave power level and electric conductivity and surface tension during microwave heating of a liquid layer have not been systematically studied.

Generally the variation of the microwave power level and change of an electric conductivity during microwave heating of a liquid layer could change the degree of penetration and rate of heat generation within the liquid layer. The reflection rate of microwave strongly depends on the

electric conductivity of the heating layer so that the effects of dielectric properties and the variation of microwave power level must be considered in this work.

Furthermore, during microwave heating, the local heating on the liquid surface by microwave causes the difference of surface tension on the surface layer and leads to the flow due to the difference of surface tension, so that the influence of surface tension effect must be clarified in detail.

This study reports a comparison of numerical predictions based on a two-dimensional model with experimental data in which the microwave of  $TE_{10}$  mode operating at a frequency of 2.45 GHz is employed.

Additionally, the application of microwave heating is largely divided into two types, conventional ovens and wave guides. The conventional microwave oven is very popular but the great number of reflections that occur make handling of the electromagnetic fields in the system very difficult. In contrast to the conventional oven, the rectangular wave guide with a constant cross-section having dimensions at least one-fourth the operating wavelength leads to have a plane wave incident on the surface of the sample. This phenomenon explains why the rectangular wave guide type is used for this work.

## 2. Experimental apparatus

Fig. 1 shows the experimental apparatus for the microwave heating system. It was a monochromatic wave of  $TE_{10}$  mode operating at a frequency of 2.45 GHz. The microwave was generated using magnetron (MICRO DENSHI., model UM-1500). It is transmitted along the  $z$ -direction of the rectangular wave guide with inner dimensions of  $109.22 \times 54.61$  mm $^2$  toward a water load that is situated at the end of the wave guide. The water load (lower absorbing

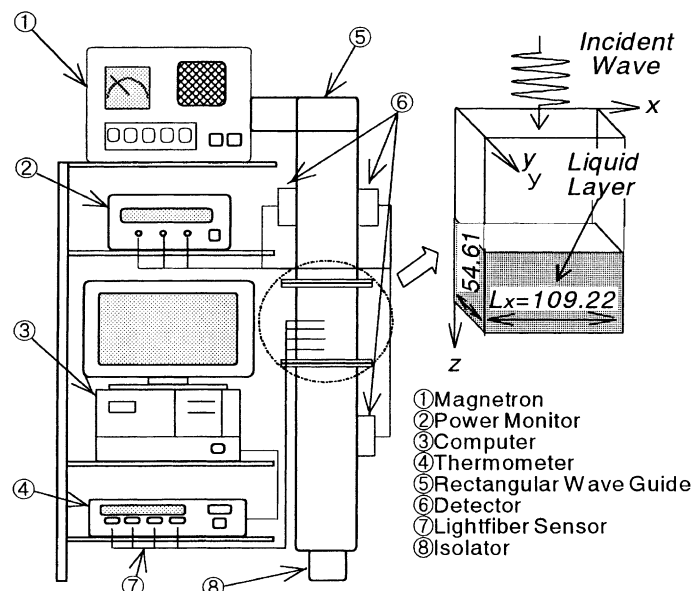


Fig. 1. Experimental apparatus.

boundary) ensures that only a minimal amount of microwave is reflected back to the sample, while an upper absorbing boundary, which is located at the end of wave guide, is used to trap any microwave reflected from the sample to prevent it from damaging the magnetron.

The powers of incident, reflected and transmitted waves were measured by wattmeter using a directional coupler (Micro Denshi Co., model DR-5000). The sample studied is a liquid layer with a thickness of 50 mm, and it is inserted in the rectangular wave guide. A container is made of polypropylene of 0.75 mm in thickness. The distributions of temperature within the sample were measured using light fiber sensors (LUXTRON Fluroptic Thermometer., Model 790, accurate to  $\pm 0.5^\circ\text{C}$ ), which were placed in the center of the sample at each 5 mm interval. An infrared camera is also used to measure the distributions of temperature within the sample in  $x-z$  plane.

### 3. The dielectric properties

The problem of microwave heating is directly related to electromagnetic fields, the temperature distribution within a dielectric material. Therefore, knowing the dielectric properties is essential for a theoretical prediction. An accurate evaluation of the electromagnetic fields, which determines microwave power dissipation within the dielectric material, is very important and crucial for the whole process. The microwave power dissipation represents the microwave power absorbed, which is eventually converted into thermal energy in dielectric materials (i.e., it represents the local electromagnetic heat generation in the materials). At the same time, the temperature will result in changes in dielectric properties. On the other hand, the dielectric properties will affect the microwave energy dissipation, thus effect variation of the temperature distribution.

In this work the pure water and NaCl-water solution layers are selected as the sample. The expressions of dielectric properties (relative permittivity  $\epsilon_r$  and dielectric loss coefficient  $\tan \delta$ ) of the sample are defined as

*Pure water.* The frequency dependence of the dielectric properties of pure water is given by the well-known Debye equation:

$$\epsilon_{rw} = \epsilon_{rwH} + \frac{\epsilon_{rwL} - \epsilon_{rwH}}{1 + \omega^2 \tau_w^2}, \quad (1)$$

$$\tan \delta_w = \frac{(\epsilon_{rwL} - \epsilon_{rwH})\omega \tau_w}{\epsilon_{rwL} + \epsilon_{rwH}\omega^2 \tau_w^2}, \quad (2)$$

where

- $\epsilon_{rwL}$  static dielectric constant of pure water (dimensionless)
- $\epsilon_{rwH}$  high frequency limit of  $\epsilon_{rw}$  (dimensionless)
- $\tau_w$  relaxation time of pure water (s)
- $\omega$  angular frequency (rad/s)

*NaCl-water solution.* The dielectric properties of NaCl-water solution are given by Stogryn:

$$\epsilon_{rb} = \epsilon_{rwH} + \frac{\epsilon_{rbL} - \epsilon_{rwH}}{1 + \omega^2 \tau_b^2}, \quad (3)$$

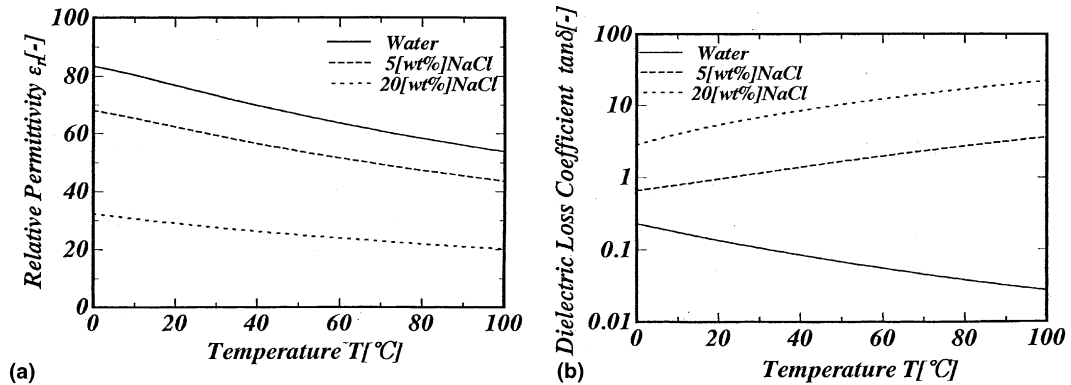


Fig. 2. Dielectric properties at different conditions used in the calculations: (a) relative permittivity; (b) dielectric loss coefficient.

$$\tan \delta_b = \left\{ \frac{(\epsilon_{rbL} - \epsilon_{rwH})\omega\tau_b}{\epsilon_{rwL} + \epsilon_{rwH}\omega^2\tau_b^2} + \frac{\sigma}{\omega\epsilon_0} \right\} / \epsilon_{rb}, \quad (4)$$

where the subscript b refers to the NaCl-water solution,  $\sigma$  is the electric conductivity of the NaCl-water solution, and  $\epsilon_0$  is the permittivity of free space.

Based on the above expressions, all dielectric properties used for the calculations are presented in Fig. 2. It is seen that the dielectric properties strongly depend on the temperature and electric conductivity (which corresponds to the percentage by weight of NaCl in solution) of the liquid layer.

#### 4. Mathematical model formulation

Generally, studies on the microwave heating involve solutions of the equations governing electromagnetic propagation, i.e., Maxwell's equations, either by themselves or coupled with the heat and momentum equations. Fig. 3 shows the analytical model for microwave heating of a liquid layer using a rectangular wave guide. In this study, the two kinds of samples, water layer and NaCl-water solution layer, are chosen to illustrate the characteristics of microwave heating.

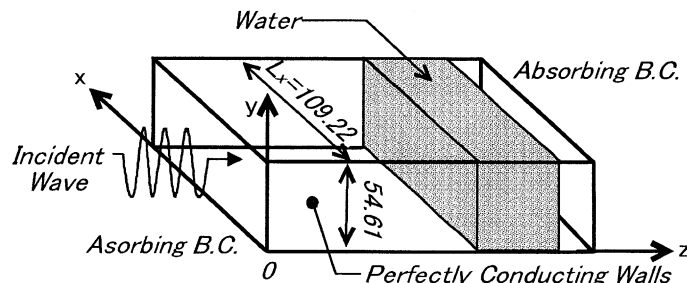


Fig. 3. Analytical model.

The surface of the sample is exposed to the microwave. Microwave in the form of plane wave is incident on this surface. Other surfaces are insulated and the heat and mass fluxes are set equal to zero.

#### 4.1. Analysis of electromagnetic field

**Assumptions.** A two-dimensional analytical model over the  $x-z$  plane in Fig. 3 is presented. The proposed model is based on the following assumptions:

- since the microwave field in the  $\text{TE}_{10}$  mode has no variation of field in the direction between the broad faces, a two-dimensional model over the  $x-z$  plane is applicable to the analysis of electromagnetic field inside a rectangular wave guide [10];
- the absorption of microwave energy by the cavity (including air) in the rectangular wave guide is negligible;
- the walls of a rectangular wave guide are perfect conductors;
- the effect of the sample container on the electromagnetic field can be neglected.

The basic equations governing the electromagnetic field vectors are based on the well-known Maxwell curl relation. The differential form of Maxwell's equation can be expressed in terms of electric field intensity  $E$  and magnetic field intensity  $H$ . Maxwell's equations describing their space and time dependence are

$$\nabla \times \vec{E} = -\frac{\partial \vec{B}}{\partial t}, \quad (5)$$

$$\nabla \times \vec{H} = \vec{J} + \frac{\partial \vec{D}}{\partial t}, \quad (6)$$

$$\nabla \cdot \vec{D} = q, \quad (7)$$

$$\nabla \cdot \vec{B} = 0, \quad (8)$$

where  $E$  and  $H$  are the electric and magnetic fields,  $J$  is the current density,  $D$  is the flux density, and  $B$  is the magnetic flux density. The constitutive relations relating  $J$ ,  $D$  and  $B$  to  $E$  and  $H$  are

$$\vec{J} = \sigma \vec{E}, \quad (9)$$

$$\vec{D} = \epsilon \vec{E}, \quad (10)$$

$$\vec{B} = \mu \vec{H}, \quad (11)$$

where  $\sigma$  is the electric conductivity,  $\mu$  is the magnetic permeability and  $\epsilon$  is the electrical permittivity. Substituting Eqs. (9)–(11), Eqs. (5)–(8) becomes

$$\nabla \times \vec{E} = -\mu \frac{\partial \vec{H}}{\partial t}, \quad (12)$$

$$\nabla \times \vec{H} = \sigma \vec{E} + \varepsilon \frac{\partial \vec{E}}{\partial t}, \quad (13)$$

$$\nabla \cdot \vec{E} = \frac{q}{\varepsilon}, \quad (14)$$

$$\nabla \cdot \vec{H} = 0. \quad (15)$$

The curl relations, Eqs. (12) and (13), are referred to Faraday's law and Ampere's law, respectively. The divergence equations, Eqs. (14) and (15), are statements of Gauss's law. The curl operator in Maxwell's equation is a measure of the field rotation. Thus Eq. (12) indicated that a time-varying electric flux generates a magnetic field with rotation, Eq. (14) states that the divergence of electric flux at a point is proportional to the position charge density and Eq. (15) states that there is no source or sink of magnetic flux.

For the microwave of TE<sub>10</sub> mode, the components of electric and magnetic field intensities are given by

$$E_x = E_z = H_y = 0, \quad (16)$$

$$E_y, H_x, H_z \neq 0, \quad (17)$$

where subscripts  $x$ ,  $y$  and  $z$  represent the  $x$ ,  $y$  and  $z$  components of vectors, respectively. Using the relations of Eqs. (16) and (17), the governing equations (Eqs. (12)–(15)) can be written in terms of the component notations of electric and magnetic field intensities:

$$\frac{\partial E_y}{\partial z} = \mu \frac{\partial H_x}{\partial t}, \quad (18)$$

$$\frac{\partial E_y}{\partial x} = -\mu \frac{\partial H_z}{\partial t}, \quad (19)$$

$$-\left(\frac{\partial H_z}{\partial x} - \frac{\partial H_x}{\partial z}\right) = \sigma E_y + \varepsilon \frac{\partial E_y}{\partial t}, \quad (20)$$

where the permittivity  $\varepsilon$ , magnetic permeability  $\mu$  and electric conductivity  $\sigma$  are given by

$$\varepsilon = \varepsilon_0 \varepsilon_r, \quad (21)$$

$$\mu = \mu_0 \mu_r, \quad (22)$$

$$\sigma = 2\pi f \varepsilon \tan \delta. \quad (23)$$

In this work, the dielectric properties are assumed to vary with temperature and percentage by weight of NaCl during the heating process.

*Boundary conditions.* Corresponding to the analytical model shown in Fig. 3, the boundary conditions can be given as follows:

(a) *Perfectly conducting boundaries.* Boundary conditions on the inner wall surface of a rectangular wave guide are given by using Faraday's law and Gauss' theorem:

$$E_t = 0, \quad H_n = 0, \quad (24)$$

where subscripts  $t$  and  $n$  denote the components of tangential and normal directions, respectively.

(b) *Continuity boundary condition.* Boundary conditions along the interface between different materials, for example, between air and dielectric material surface, are given by using Ampere's law and Gauss' theorem:

$$\begin{aligned} E_t &= E'_t, \quad H_t = H'_t, \\ D_n &= D'_n, \quad B_n = B'_n. \end{aligned} \quad (25)$$

(c) *Absorbing boundary condition.* At both ends of the rectangular wave guide, the first-order absorbing conditions proposed by Mur [14] are applied:

$$\frac{\partial E_y}{\partial t} = \pm v \frac{\partial E_y}{\partial z}. \quad (26)$$

Here, the symbol  $\pm$  represents the forward or backward waves and  $v$  is the phase velocity of the propagation wave.

(d) *Oscillation of the electric and magnetic field intensities by magnetron.* Incident wave due to magnetron is given by the following equations:

$$E_y = E_{y\text{in}} \sin \left( \frac{\pi x}{L_x} \right) \sin (2\pi ft), \quad (27)$$

$$H_x = \frac{E_{y\text{in}}}{Z_H} \sin \left( \frac{\pi x}{L_x} \right) \sin (2\pi ft), \quad (28)$$

where  $E_{y\text{in}}$  is the input value of electric field intensity,  $L_x$  is the length of the rectangular wave guide in the  $x$ -direction,  $Z_H$  is the wave impedance defined as

$$Z_H = \frac{\lambda_g Z_I}{\lambda} = \frac{\lambda_g}{\lambda} \sqrt{\frac{\mu}{\epsilon}}, \quad (29)$$

where  $Z_I$  denotes intrinsic impedance depending on the properties of the material.  $\lambda$  and  $\lambda_g$  are the wave lengths of microwaves in free space and rectangular wave guide, respectively.

The power flux associated with a propagating electromagnetic wave is represented by the Poynting vector:

$$S = \frac{1}{2} \operatorname{Re}(E \times H^*) \quad (30)$$

The Poynting theorem allows the evaluation of the microwave power input. It is expressed as

$$P_{\text{in}} = \int_A S dA = \frac{A}{4Z_H} E_{y\text{in}}^2. \quad (31)$$

#### 4.2. Heat transport and fluid flow equations

A schematic diagram of the model is shown in Fig. 3. In order to reduce complexity of the phenomena, several assumptions have been introduced into the heat and fluid flow equations:

- corresponding to electromagnetic field, temperature field also can be assumed to be two-dimensional plane ( $x-z$  plane),

- the surroundings of the liquid layer sample are insulated except at the upper surface where energy exchanges with the ambient air,
- the effect of the container on temperature and flow fields can be neglected,
- the effect of the phase change for liquid layer can be neglected,
- liquid layer is assumed when the Boussinesq approximation is valid.

#### 4.2.1. Heat transport equations

The temperature of the liquid layer exposed to incident wave is obtained by solving the conventional heat transport equation with the microwave power absorbed included as a local electromagnetic heat generation term:

$$\frac{\partial T}{\partial t} + u \frac{\partial T}{\partial x} + w \frac{\partial T}{\partial z} = \alpha \left( \frac{\partial^2 T}{\partial x^2} + \frac{\partial^2 T}{\partial z^2} \right) + \frac{Q}{\rho C_p}. \quad (32)$$

where  $Q$  is the local electromagnetic heat generation term, which is a function of the electric field and defined as

$$Q = 2\pi f \varepsilon_0 \varepsilon_r (\tan \delta) E_y^2, \quad (33)$$

where  $\varepsilon_r$  denotes the relative dielectric constant and  $\varepsilon_0$  denotes the permittivity of free space.

#### 4.2.2. The fluid flow equations

The generalized sets of two-dimensional governing equations for a Newtonian Boussinesq fluid are given as

continuity equation:

$$\frac{\partial u}{\partial x} + \frac{\partial w}{\partial z} = 0, \quad (34)$$

$x$ -momentum equation:

$$\frac{\partial u}{\partial t} + u \frac{\partial u}{\partial x} + w \frac{\partial u}{\partial z} = -\frac{1}{\rho} \frac{\partial p}{\partial x} + v \left( \frac{\partial^2 u}{\partial x^2} + \frac{\partial^2 u}{\partial z^2} \right), \quad (35)$$

$y$ -momentum equation:

$$\frac{\partial w}{\partial t} + u \frac{\partial w}{\partial x} + w \frac{\partial w}{\partial z} = -\frac{1}{\rho} \frac{\partial p}{\partial z} + v \left( \frac{\partial^2 w}{\partial x^2} + \frac{\partial^2 w}{\partial z^2} \right) + g\beta(T - T_\infty), \quad (36)$$

where  $v$  and  $\beta$  are the kinematics viscosity and coefficient of thermal expansion of the liquid layer, respectively.

#### 4.2.3. Boundary and initial conditions

Relative to the coordinate system as shown in Fig. 3, the appropriate boundary conditions for solving system of Eqs. (32)–(36) are valid for a liquid layer as well as the walls of container. Since the walls of container are rigid, the velocities are zero. Considering the governing equations (32)–(36) are subjected to the following boundary conditions. At the interfaces between liquid layer and the walls of container, zero slip boundary conditions are used for the momentum equations. At

the upper surface, the velocity in the normal direction ( $w$ ) and shear stress in the horizontal direction are assumed to be zero, where the influence of Marangoni flow can be applied:

$$\eta \frac{\partial u}{\partial z} = - \frac{d\xi}{dT} \frac{\partial T}{\partial x}, \quad (37)$$

where  $\eta$  and  $\xi$  are the absolute viscosity and surface tension of the liquid layer, respectively.

The boundary conditions proposed for the upper surface of the liquid layer, where heat is lost from the surface via natural convection and radiation:

$$-\lambda \frac{\partial T}{\partial z} = h_c(T - T_\infty) + \sigma_{\text{rad}}\varepsilon_{\text{rad}}T^4 \quad (38)$$

where  $h_c$  is the local heat transfer coefficient,  $\sigma_{\text{rad}}$  is the Stefan–Boltzmann constant and  $\varepsilon_{\text{rad}}$  is the radiative surface emissivity of materials.

Consider the boundary conditions at the closed boundary (adiabatic-impermeable) when no heat and mass exchanges take place:

$$\frac{\partial T}{\partial x} = \frac{\partial T}{\partial z} = 0. \quad (39)$$

The initial condition of a liquid layer is defined as

$$T = T_0 \quad \text{at } \mathbf{t} = \mathbf{0}. \quad (40)$$

## 5. Numerical solution procedure

The description of heat and fluid flow equations (Eqs. (32)–(36)) requires specification of two velocity components ( $u, w$ ), one fluid pressure ( $p$ ) and the temperature ( $T$ ) in a liquid layer. These equations are coupled to the Maxwell equations (Eqs. (18)–(20)) by Eq. (33). The latter equation represents the heating effect of microwaves in the liquid layer. The numerical schemes of the microwave heating process are performed.

### 5.1. Electromagnetic field equations and FDTD discretization

Generally, simulation of microwave power dissipation requires the solution of the set of three coupled scalar partial differential equations governing electromagnetic propagation, i.e., Maxwell's equation, inside a rectangular wave guide. The finite difference time-domain (FDTD) method has been used to provide a full description of electromagnetic scattering and absorption and give detailed spatial and temporal information of wave propagation.

In this study, the leapfrog scheme is applied to a set of Maxwell's equations. The electric field vector components are offset one half cell in the direction of their corresponding components, while the magnetic field vector components are offset one half cell in each direction orthogonal to their corresponding components [15]. The electric and magnetic fields are evaluated at alternative half time steps. For TE mode, the electric and magnetic field components are expressed by the total field FDTD equations as

$$E_y^n(i, k) = \frac{1 - \frac{\sigma(i, k)\Delta t}{2\varepsilon(i, k)}}{1 + \frac{\sigma(i, k)\Delta t}{2\varepsilon(i, k)}} E_y^{n-1}(i, k) + \frac{1}{1 + \frac{\sigma(i, k)\Delta t}{2\varepsilon(i, k)}} \frac{\Delta t}{\varepsilon(i, k)} \left\{ \frac{-(H_z^{n-1/2}(i + 1/2, k) - H_z^{n-1/2}(i - 1/2, k))}{\Delta x} \right. \\ \left. + \frac{(H_x^{n-1/2}(i + 1/2, k) - H_x^{n-1/2}(i - 1/2, k))}{\Delta z} \right\}, \quad (41)$$

$$H_x^{n+1/2}(i, k + 1/2) = H_x^{n-1/2}(i, k + 1/2) + \frac{\Delta t}{\mu(i, k + 1/2)} \left\{ \frac{E_y^n(i, k + 1) - E_y^n(i, k)}{\Delta z} \right\}, \quad (42)$$

$$H_z^{n+1/2}(i + 1/2, k) = H_z^{n-1/2}(i + 1/2, k) - \frac{\Delta t}{\mu(i + 1/2, k)} \left\{ \frac{E_y^n(i + 1, k) - E_y^n(i, k)}{\Delta x} \right\}. \quad (43)$$

## 5.2. Heat transport and fluid flow equations and finite control volume discretization

The coupled non-linear set of Eqs. (32)–(40) is solved numerically by using the finite control volume method base on the SIMPLE algorithm developed by Patankar [16]. The advantage of this method is that it ensures flux conservation, and thus avoids generation of parasitic sources, which leads to the solution which is sufficiently converged. The basic strategy of the finite control volume discretization method is to divide the calculated domain into a number of control volumes and then integrate the conservation equations over this control volume over an interval of time  $[t, t + \Delta t]$ . At the boundaries of the calculated domain, the conservation equations are discretized by integrating over half the control volume and by taking into account the boundary conditions. At the corners of the calculated domain we used a quarter of control volume. The fully implicit time discretization finite difference scheme is used to arrive at the solution in time. Additionally, the details about numerical discretization of this method can be found in the recent literature [16].

## 5.3. The stability and accuracy of calculation

The choice of spatial and temporal resolution is motivated by reasons of stability and accuracy. Spatially, as shown in Fig. 4, Eqs. (41)–(43) are solved on a grid system, and temporally they are solved alternatively for both the electric and magnetic fields. To insure stability of the time-stepping algorithm  $\Delta t$  must be chosen to satisfy the courant stability condition and defined as

$$\Delta t \leq \frac{\sqrt{(\Delta x)^2 + (\Delta z)^2}}{v} \quad (44)$$

and the spatial resolution of each cell, defined as

$$\Delta x, \Delta z \leq \frac{\lambda_g}{10\sqrt{\varepsilon_r}}, \quad (45)$$

where  $v$  is the velocity of an electromagnetic wave.

Corresponding to Eqs. (44) and (45), the calculation conditions are as follows:

- grid size:  $dx = dz = 1.0922$  mm,

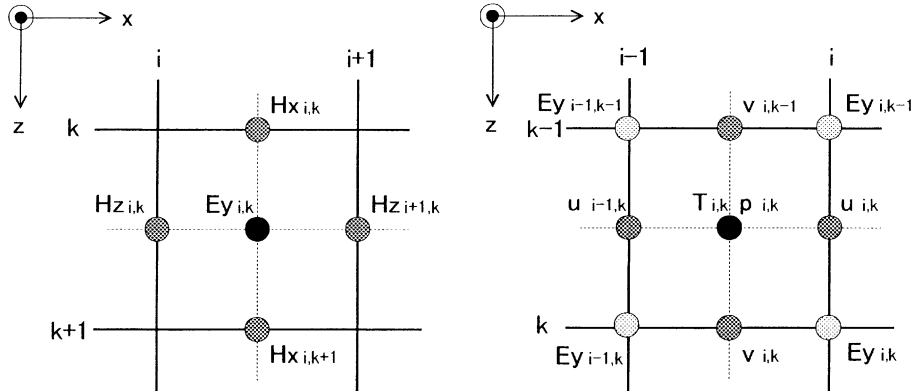


Fig. 4. Grid system configuration.

- since the propagating velocity of microwave is so fast compared with the rate of heat transfer, different time steps of  $\Delta t = 2 \times 10^{-12}$  s and  $\Delta t = 0.01$  s are used corresponding to electromagnetic field and temperature field calculations, respectively,
- number of grids:  $N = 100$  (width)  $\times 200$  (length),
- relative error in the iteration procedures of  $10^{-8}$  were chosen.

#### 5.4. The iterative computational schemes

Since the dielectric properties of liquid layer samples are temperature dependent, to understand the influence of electromagnetic field on microwave heating of liquid layer realistically it is necessary to consider the coupling between electric field and temperature and fluid flow fields. For this reason, the iterative computational schemes are required to resolve the coupled non-linear Maxwell's equations, momentum and heat transport equations.

The computational scheme is to first compute a local heat generation term by running an electromagnetic calculation with uniform properties determined from initial temperature data. The electromagnetic calculation is performed until a sufficient period is reached in which a representative average rms (root-mean-square) of the electric field at each spatial point is obtained, typically 30 000 time steps. The microwave power absorption at each point is computed and used to solve the time dependent temperature and velocities fields. Using these temperatures new values of the dielectric properties are calculated and used to re-calculate the electromagnetic fields and then the microwave power absorption. All the steps are repeated until the required heating time is reached. The details of computational schemes and strategy are illustrated in Fig. 5.

## 6. Results and discussion

The experimental results for microwave heating of liquid layers (water and NaCl-water solution layer) were compared with mathematical model simulations. In order to test the validity of the mathematical model, the results are divided into two parts that cover: part one is the simulation of electric field inside a rectangular wave guide and liquid layer. The other part shows the results of

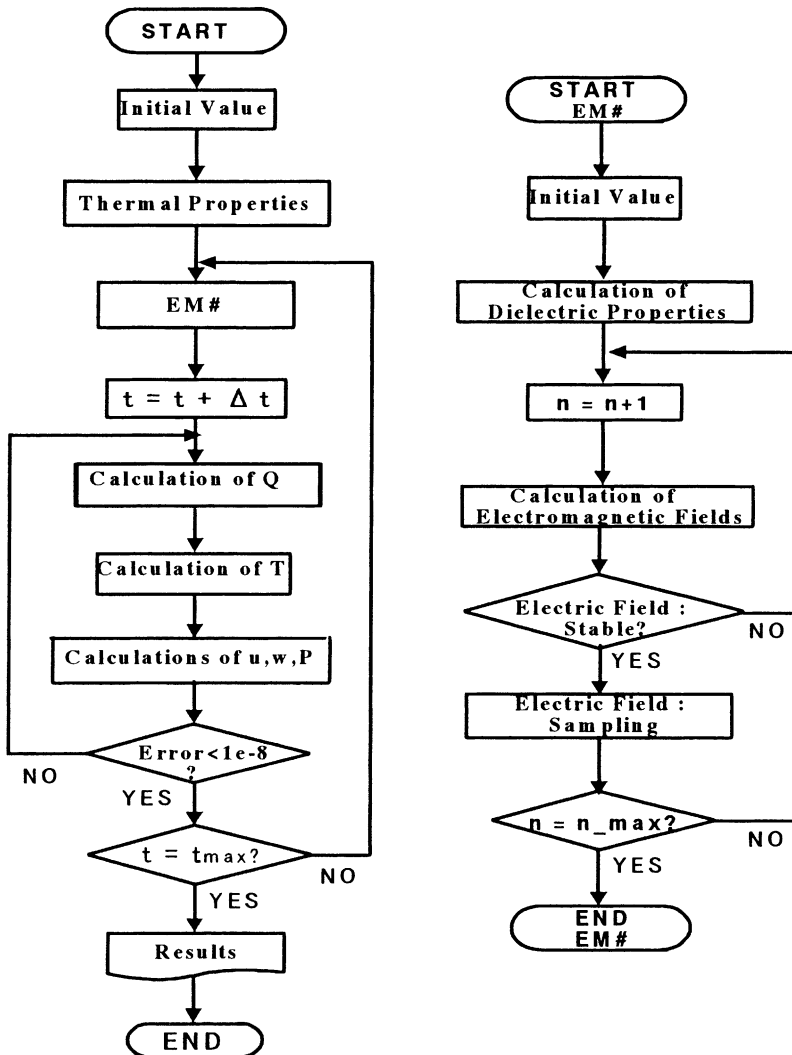


Fig. 5. Computational schemes (EM#: subroutine for calculation of electromagnetic fields; n: calculation loop of electromagnetic field).

the distribution of temperature and velocity fields within the liquid layer. However, all processes using the two levels of microwave power level (300 and 1000 W) were distinguished. One aspect of model verification was to compare the heating data from experiments run under different conditions with mathematical calculations using parameter values obtained from Table 1.

### 6.1. Simulation of electric field inside a rectangular wave guide

To understand the electrical field inside the rectangular wave guide and the liquid layer, simulation analysis is required. In Figs. 6 and 7 are the simulated electric fields of TE<sub>10</sub> mode along

Table 1

The electromagnetic and thermo physical properties used in the computations

$\epsilon_0 = 8.85419 \times 10^{-12}$ (F/m)	$\mu_0 = 4.0\pi \times 10^{-7}$ (H/m)
$\epsilon_{ra} = 1.0$	
$\mu_{ra} = 1.0$	$\mu_{rw} = 1.0$
$\tan \delta_a = 0.0$	
$\rho_a = 1.205$ (kg/m <sup>3</sup> )	$\rho_w = 1000.0$ (kg/m <sup>3</sup> )
$c_{pa} = 1.007$ (kJ/(kg K))	$c_{pw} = 4.186$ (kJ/(kg K))

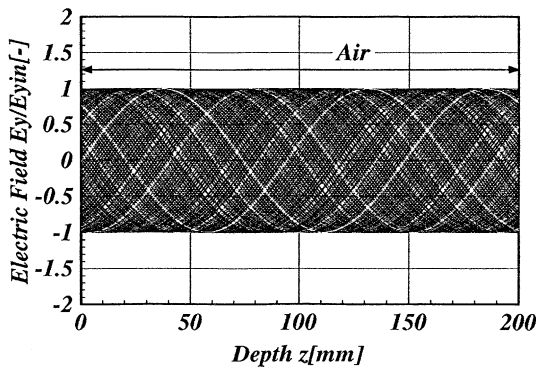


Fig. 6. Distribution of electric field in the case of a rectangular wave guide is empty.

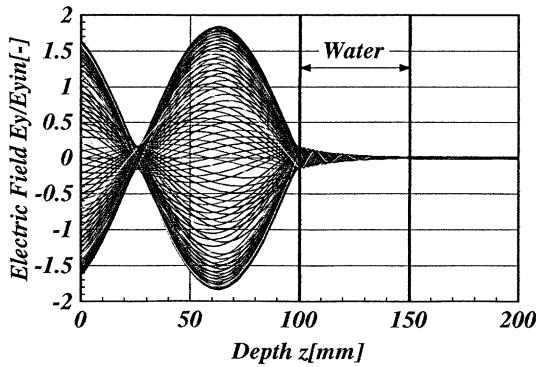


Fig. 7. Distribution of electric field in the case of a liquid layer is inserted in the rectangular wave guide.

the center axis  $x = 54.61$  of a rectangular wave guide for the case of a rectangular wave guide is empty (which corresponds to that of air) and for the case when the liquid layer is inserted in the rectangular wave guide, respectively. The vertical axis represents the intensity of the electric field  $E_y$ , which is normalized to the amplitude of the input electromagnetic wave,  $E_{yin}$ . Fig. 6 shows the static wave of TE<sub>10</sub> mode in the case of a rectangular wave guide is empty. A uniform static wave is formed inside a rectangular wave guide. In Fig. 7 shows corresponding to that case when the liquid layer is inserted in the rectangular wave guide, since the incident wave passing through the cavity having low permittivity is directly irradiated with the sample having high permittivity, a

major part of incident wave is reflected from the surface of the sample and a stronger standing wave with a larger amplitude forms in the cavity forward to the liquid layer while the electric field within the sample is extinguished. However, the electric field distribution for the case of NaCl-water solution layer, a stronger standing wave with a larger amplitude forms within the layer. Since the electric conductivity of a NaCl-water solution layer is significantly higher than that of a water layer.

## 6.2. The distribution of temperature and velocity fields within a liquid layer

### 6.2.1. Microwave heating of water layer

Figs. 8 and 9 show the comparison for the temperature distribution within the water layer between the predicted and experimental results at various times, along with the horizontal axis ( $z = 5 \text{ mm}$ ) and vertical axis ( $x = 54.61 \text{ mm}$ ) of a rectangular wave guide, respectively, which correspond to those of initial temperature with  $0^\circ\text{C}$  and microwave power level of 300 W.

In Fig. 8, the result shows the greatest temperature in the center of heating layer with the temperature decreasing towards the side walls of the water layer.

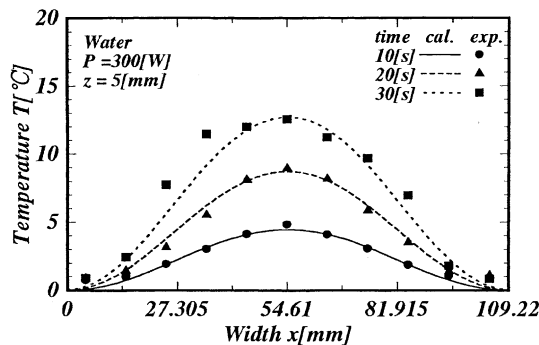


Fig. 8. Distribution of temperature within a water layer as a function of distance at various times ( $P = 300 \text{ W}$ ,  $z = 5 \text{ mm}$ ).

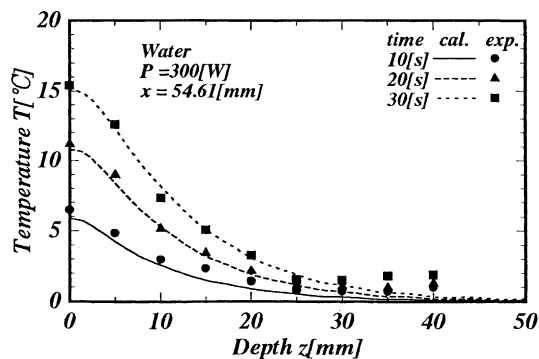


Fig. 9. Distribution of temperature within water layer as a function of distance at various times ( $P = 300 \text{ W}$ ,  $x = 54.61 \text{ mm}$ ).

In Fig. 9, the temperature within the water layer closest to the incoming microwave is shown. This region heats up to a higher level at a faster rate than elsewhere within the liquid layer. Nevertheless, the temperature decays slowly along the propagation direction because of the skin-depth heating effect. The predicted results are in agreement with the experimental results for the microwave heating.

Fig. 10 depicts the velocity fields within water layer at various times. At the early stage of heating (left-hand side of Fig. 10), the effect of convection plays the smallest role where the heat transfer occurs primarily by the conduction mode. As the heating proceeds, the local heating on the surface of water layer causes the difference of surface tension on the surface of water layer, which leads to the convective flow of water (Marangoni flow). This causes water to flow from the hotter region (higher power absorbed) at the middle of water layer to the cold region (lower power absorbed) at the side walls of the container (right-hand side of Fig. 10). In this stage of heating, the effect of convective flow becomes stronger and plays a more important role, especially at the upper portion of the side walls of container. However, at the bottom region of the walls where the convection plays the smallest, temperature distributions are still primarily by the conduction mode.

Figs. 11 and 12 show the distribution of temperature fields for the microwave power levels of 300 and 1000 W, respectively, along with the horizontal axis ( $z = 5 \text{ mm}$ ) of a rectangular wave guide. By comparing Fig. 11 with Fig. 12, it is seen that the temperature field within the water layer in the case of  $P = 1000 \text{ W}$  is significantly greater than that of  $P = 300 \text{ W}$ . The distributions of temperature field near the middle region of water layer tends to be uniformed, because the strong effect of Marangoni flow causes the hot spot to move from the middle region to the side walls of the container, especially, at the end stage of heating.

Additionally, Figs. 11 and 12 show that the temperature within the water layer rises up quickly in the early stage of heating. After this it rises the slowdown with elapsed times, due to the behavior of the dielectric loss coefficient which decreases significantly with increasing temperature. As referred to Fig. 2, the microwave power absorbed can decrease at locations of higher

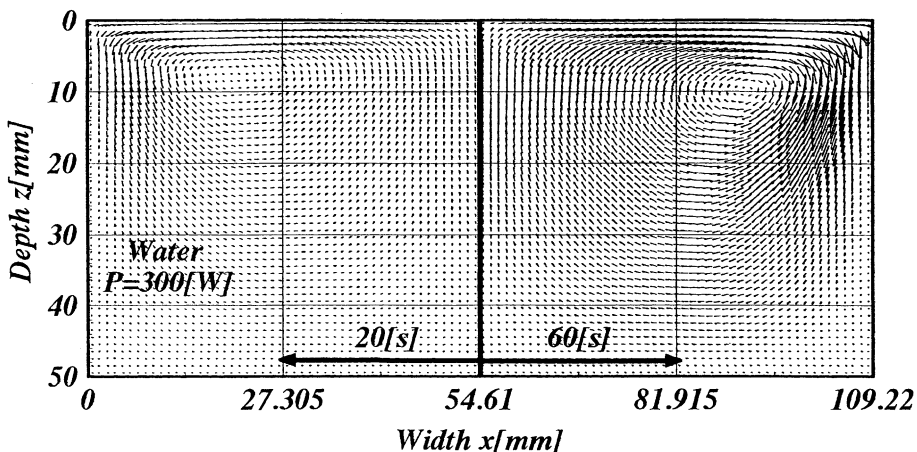


Fig. 10. Flow field patterns within water layer at various times.

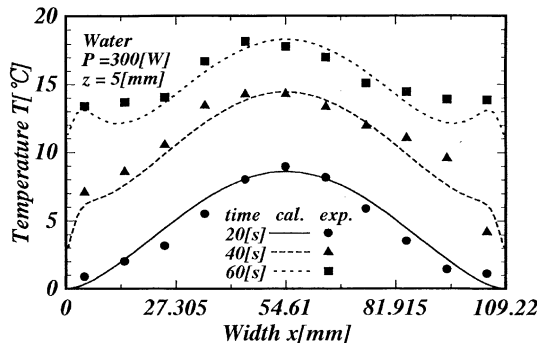


Fig. 11. Distributions of temperature within water layer as a function of distance at various times ( $P = 300$  W,  $z = 5$  mm).

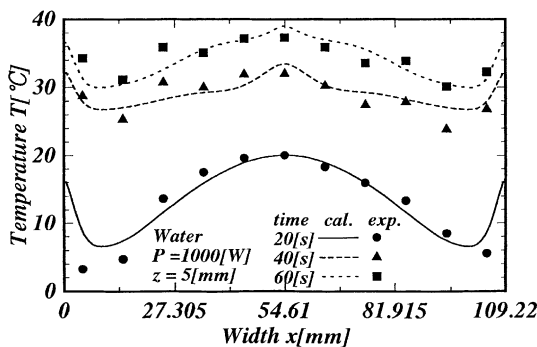


Fig. 12. Distributions of temperature within water layer as a function of distance at various times ( $P = 1000$  W,  $z = 5$  mm).

temperature where the standing wave configuration established within the liquid layer minimizes. The predicted results are in agreement with the experimental results for the microwave heating.

The prediction and experimental data of temperature distribution within the water layer in the vertical plane ( $x-z$ ) with heating time of 60 s are compared in Figs. 13 and 14, which correspond to those of microwave power levels of 300 and 1000 W, respectively. The result shows the greatest temperature in the upper region of heating sample with the temperature decreasing towards the lower wall. It can be seen that the agreement between the two heating patterns is good, particularly concerning the location of the hot region.

In the case of microwave power level of 300 W (Fig. 13), the temperature within the water layer closest to the incoming microwave and the temperatures have a trend corresponding to those of velocity fields. This region heats up to a higher level at a faster rate than elsewhere within the water layer.

In the case of microwave power level of 1000 W (Fig. 14), most of the heating takes place inside the water layer. This is because of the skin-depth heating effect, which increases a larger part of the incident wave can penetrate further into the sample compared with the case of microwave level of 300 W.

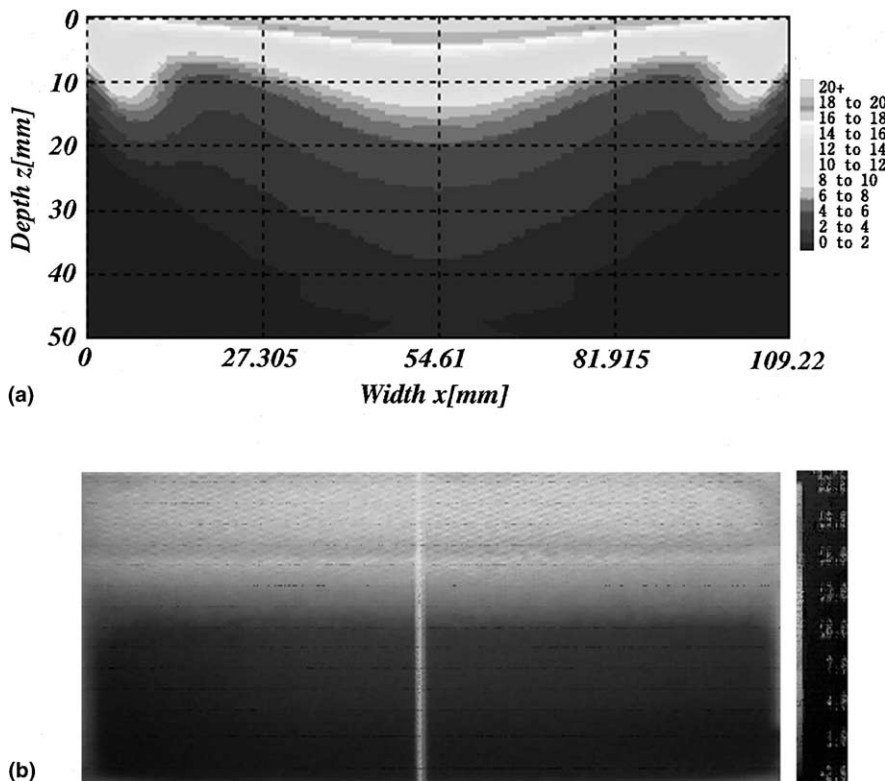


Fig. 13. Comparison between predicted result (a) and experimental result (b) for microwave heating of water layer ( $P = 300$  W,  $t = 60$  s).

#### 6.2.2. Microwave heating of NaCl-water solution layer

This section is performed to examine the characteristic of a microwave heating of NaCl-water solution layer inside a rectangular wave guide as a parameter of the electric conductivity (which corresponds to the percentage by weight of NaCl in liquid layer) and microwave power level.

Fig. 15 shows the distribution of temperature field in a NaCl-water solution layer, which corresponds to those of initial temperature with 0 °C, 5% of NaCl, heating time of 60 s and microwave power level of 300 W, respectively.

Since the electric conductivity of NaCl-water solution layer is significantly higher than those of a water layer, the higher electric conductivity leads to much a larger dielectric loss coefficient ( $\tan \delta$ ). Consequently, most of the power absorbed is more intensely close to the leading edge of liquid layer where resulting in a thinner thermally stratified layer.

Figs. 16(a) and (b) show the comparison of the velocity and temperature fields for the microwave heating of the water layer and NaCl-water solution layer, respectively, which correspond to those of initial temperature with 0 °C, heating time of 60 s and microwave power level of 300 W.

Since the intensity of absorbed power and the heating rates for NaCl-water solution layer are significantly greater than that of water layer it leads to a stronger effect of surface tension on the

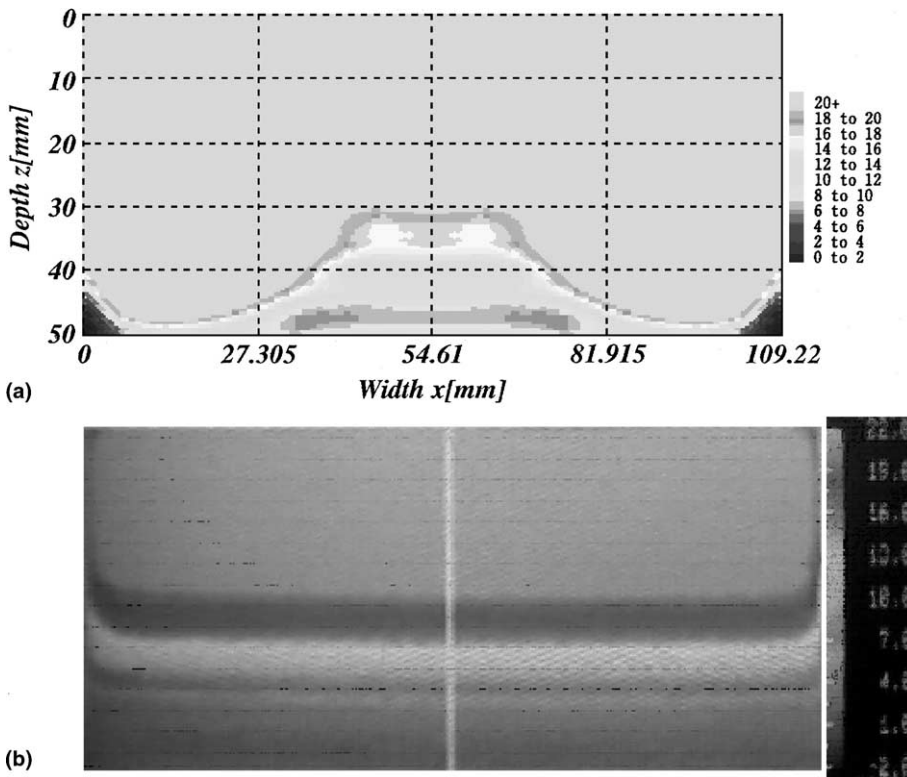


Fig. 14. Comparison between predicted result (a) and experimental result (b) for microwave heating of water layer ( $P = 1000$  W,  $t = 60$  s).

surface layer. Corresponding to this phenomenon, the effect of convective flow becomes stronger and plays a more important role, a complex velocity field associated with many convection cells is formed at the side walls of container (right-hand side of Fig. 16(a)) and resulting in a thicker thermally stratified layer near the side walls of container too (right-hand side of Fig. 16(b)).

However, at the region near the bottom of the walls convection is quite weak and conduction is still dominated by the local electromagnetic heat generation term.

Figs. 17 and 18 show the comparison for the distribution of temperature within liquid layer (water layer and NaCl-water solution layer) between the predicted and experimental results at various conditions, along with the horizontal axis ( $z = 5$  mm) and vertical axis ( $x = 54.61$  mm) of a rectangular wave guide, respectively, which corresponds to those of initial temperature with  $0^\circ\text{C}$ , heating time of 60 s and microwave power level of 300 W.

In Fig. 17 shows that in the case of NaCl-water solution layer (5% and 20% of NaCl), the distributions of temperature fields near the middle region of the heating layer tends to be uniformed because of the strong effect of surface tension on the surface of heating layer. However, in the case of higher electric conductivity (20% of NaCl), because of the higher electric conductivity of heating layer, the skin-depth heating effect causes a major part of the incident wave to be reflected from the surface during the heating. This phenomenon explains why the amplitude of

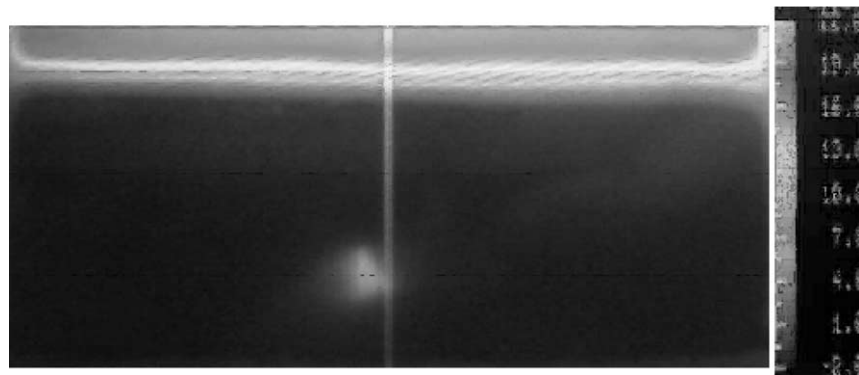


Fig. 15. Experimental result for microwave heating of NaCl-water solution layer ( $P = 300$  W,  $t = 60$  s).

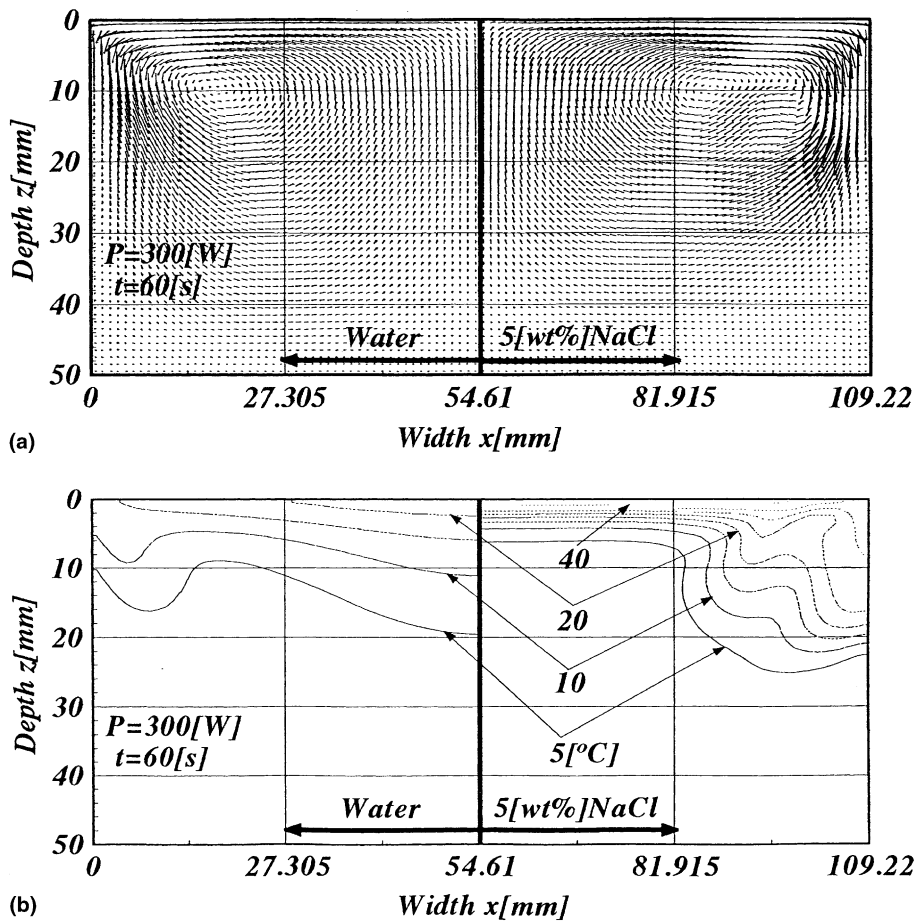


Fig. 16. Comparison of flow field patterns (a) and isotherms (b) for microwave heating of liquid layers ( $P = 300$  W,  $t = 60$  s).

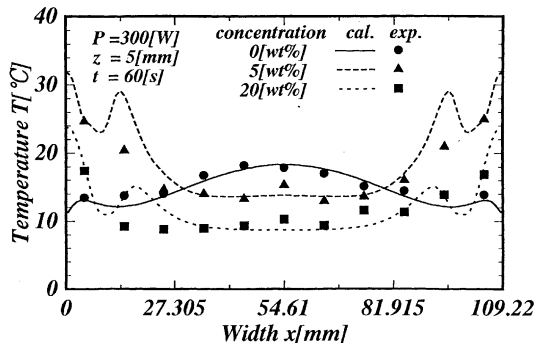


Fig. 17. Distributions of temperature within NaCl-water solution layer as a function of distance at various times ( $P = 300$  W,  $z = 5$  mm).

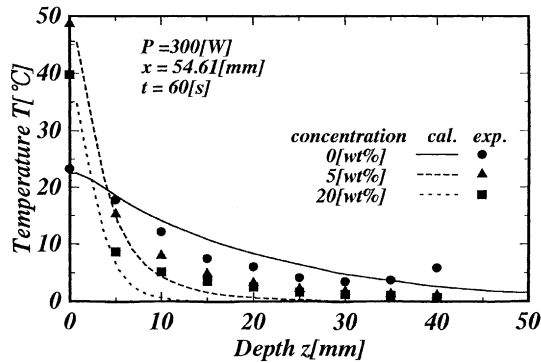


Fig. 18. Distributions of temperature within NaCl-water solution layer as a function of distance at various times ( $P = 300$  W,  $x = 54.61$  mm).

microwave inside liquid layer in the case of a higher electric conductivity (20% of NaCl) is slightly lower than that observed in that case of the lower electric conductivity (5% of NaCl) and why the heating is more intense close to the leading edge of the heating layer (Fig. 18).

Nevertheless, in the case of water layer (0% of NaCl), in contrast to that case of NaCl-water solution layer, the distribution of temperature inside ( $z > 5$  mm) the water layer is slightly higher than that observed in the case of NaCl-water solution layer (Fig. 18) and the distribution of temperature near the center of heating layer stays hotter due to the small effect of surface tension or Marangoni flow (Fig. 17). The predicted results are in agreement with the experimental results for the microwave heating of liquid layer.

#### 6.2.3. General observations of the results from prediction and experimental data during microwave heating of liquid layer

The previous section described the results from prediction and experimental data. It can be seen that the agreement between two heating patterns is almost the same, particularly concerning the

location of the hot region. However, there are some differences in the distribution of temperature between the predicted and experimental results, see Figs. 13, 14 and 18.

The observation of isotherms depicted in Figs. 13 and 14 for water layer verifies that the magnitudes of the temperatures predicted within the heating layer are all close to the experimental values. However, the complex shape of the numerical isotherms does not appear in the experimental results. This difference is thought to be caused mainly by the effect of heat loss through the walls of heating layer while taking a photograph by using an infrared camera. The distributions of temperature at selected locations within the heating layer are shown in Fig. 18. For the water layer, the prediction and experimental data agree well. However, for NaCl-water solution layer, the experimental data are significantly higher than the predicted results, especially, at the positions of  $z > 10$  mm. At this position, the experimental temperature data exceeded the predicted value near 3 °C. The discrepancy may be attributed to uncertainties in the thermal and dielectric property data base.

From this study, the capability of the mathematical model to correctly handle the field variations at the interfaces between materials of different dielectric properties was shown. With further quantitative validation of the mathematical model for a rectangular wave guide it is clear that the model can be used as a real tool for investigating in detail this particular microwave heating of liquid layer at a fundamental level.

## 7. Conclusions

The experiments and theoretical analysis presented in this paper describe many of the important interactions within a liquid layer during microwave heating using a rectangular wave guide. The following summarizes the conclusions of this work:

- A generalized mathematical model of heating process by microwave using a rectangular wave guide is proposed. It is used successfully to describe the heating phenomena of liquid layer under various conditions.
- The calculations of electromagnetic fields inside the rectangular wave guide and the liquid layer show that the variation of microwave power level and electric conductivity value changes the degree of penetration and rate of heat generation within the liquid layer. The reflection rate of microwave strongly depends on the electric conductivity value within the liquid layer.
- The distributions of temperature and velocity fields in the liquid layer correspond to the electromagnetic fields. The predicted results are in agreement with the experimental results.

## Acknowledgements

The authors gratefully acknowledge the financial support provided under the Science Research Grant of the Japanese Ministry of Education, for the development of the experimental and simulation facilities described in this paper.

## References

- [1] A.C. Metaxas, R.J. Meridith, *Industrial Microwave Heating*, Peter Peregrinus, London, 1983.
- [2] C. Saltiel, A. Datta, Heat and mass transfer in microwave processing, *Adv. Heat Transfer* 30 (1997) 1–94.
- [3] W. Li, M.A. Ebadian, T.L. White, R.G. Grubb, Heat transfer within a concrete slab applying the microwave decontamination process, *ASME J. Heat Transfer* 115 (1993) 42–50.
- [4] J. Clemens, C. Saltiel, Numerical modeling of materials processing in microwave furnaces, *Int. J. Heat Mass Transfer* 39 (8) (1996) 1665–1675.
- [5] D.C. Dibben, A.C. Metaxas, Frequency domain vs. time domain finite element methods for calculation of fields in multimode cavities, *IEEE Trans. Magn.* 33 (2) (1997) 1468–1471.
- [6] H. Zhao, I.W. Turner, The use of a coupled computational model for studying the microwave heating of wood, *Appl. Math. Modeling* 24 (2000) 183–197.
- [7] J.R. Bows, M.L. Patrick, R. Janes, A.C. Metaxas, et al., Microwave phase control heating, *Int. J. Food Sci. Technol.* 34 (1999) 295–304.
- [8] H. Zhao, I.W. Turner, G. Torgovnikov, An experimental and numerical investigation of the microwave heating of wood, *J. Microwave Power Electromagn. Energy* 33 (1998) 121–133.
- [9] J. Watanuki, Fundamental study of microwave heating with rectangular wave guide, M.S. Thesis (in Japanese), Nagaoka University of Technology, Japan 1998.
- [10] P. Ratanadecho, K. Aoki, M. Akahori, A numerical and experimental study of microwave drying using a rectangular wave guide, *Drying Technol. J.* 19 (5) (2001).
- [11] P. Ratanadecho, K. Aoki, M. Akahori, A numerical and experimental investigation of the modelling of microwave melting of frozen packed beds using a rectangular wave guide, *Int. Comm. Heat Mass Transfer* 28 (2001) 751–762.
- [12] K.G. Ayappa, S. Brandon, et al., Microwave driven convection in a square cavity, *AICHE J.* 31 (5) (1985) 842–848.
- [13] Q. Zhang, T.H. Jackson, A. Uungan, Numerical modeling of microwave induced natural convection, *Int. J. Heat Mass Transfer* 43 (8) (2000) 2141–2154.
- [14] G. Mur, Absorbing boundary conditions for the finite-difference approximation of the time-domain electromagnetic-field equations, *IEEE Trans. Electromagn. Compat. EMC-23* (4) (1981) 377–382.
- [15] K.S. Yee, Numerical solution of initial boundary value problems involving Maxwell's equation in isotropic media, *IEEE Trans. Antennas Propag. AP-14* (1966) 302–307.
- [16] S.V. Patankar, *Numerical Heat Transfer and Fluid Flow*, Hemisphere, New York, 1980.